CHAPTER V
LABORATORY TESTING

5.1 Introduction

This chapter describes geotechnical testing, including methods and results of the compaction, direct shear, and consolidation tests. Particle sizes of less than 0.25 mm (set I) are used here to mix with construction grade bentonite. Compaction tests are performed to obtain the maximum dry density and optimum water content under different mixing ratios. The specimens after compaction are used for the direct shear and consolidation testing.

5.2 Compaction test

5.2.1 Test method

The fine-grained stone dust classified in the previous chapter is mixed with bentonite using percentages of bentonite of 100, 80, 60, and 40% by weight. The mixtures are prepared in stainless steel tray using 2.7 kilograms of the mixture (Figure 5.1). Water is added to the mixture until the desired water content is reached. The components are thoroughly mixed using a spatula to ensure uniform distribution. In accordance with the ASTM D1557-12 (2021) standard method, the mixture is then compacted within the mold using a 10-pound weight dropped and released 27 times per layer for a total of five layers (Figure 5.2).

Figure 5.1 Fine-grained stone dust mixed with bentonite prepared in plastic tray.

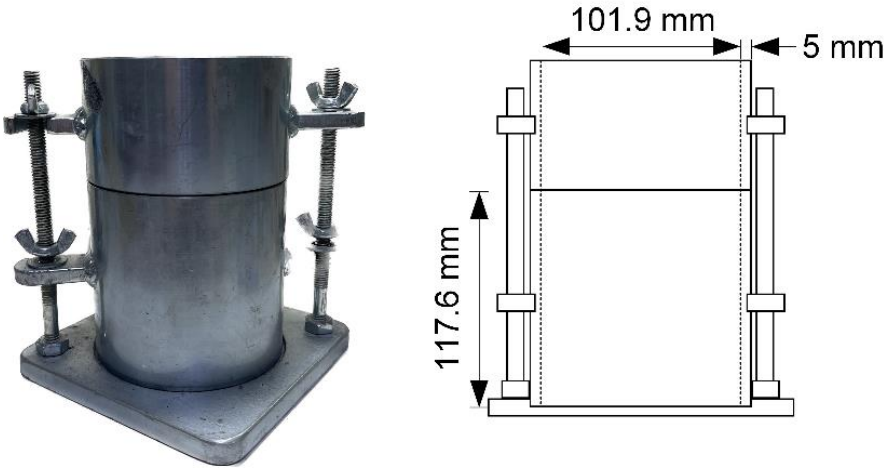

Figure 5.2 Compaction mold based on ASTM D1557-12 (2021) standard method.

5.2.2 Test results

The results show the maximum dry unit weight (ρ_{dry}) as a function of water weight ratios in Figure 5.3. The data reveals a trend of increasing maximum dry density with increasing stone dust ratios. This observation suggests that coarser mixtures achieve higher dry densities compared to finer ones. As water content is introduced, the volume of voids within the mixture increases, leading to a corresponding decrease in density (Figure 5.4). Also show the rise in maximum unit weight with increasing stone dust weight ratios, where the mixtures after compaction have higher unit weight than those before compaction. Figure 5.5 shows trend of optimum water content, which decreases as the bentonite weight ratio increases. A summary of the compaction test results is provided in Table 5.1."

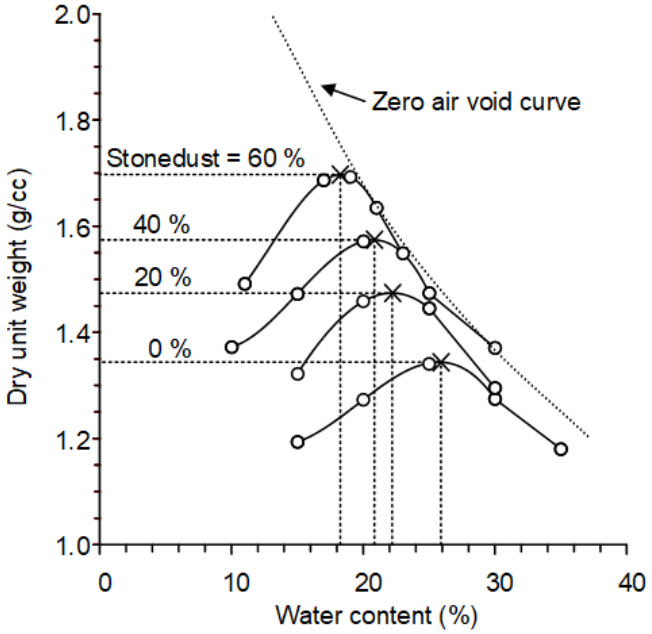

Figure 5.3 Maximum dry unit weight as a function of water content for various stone dust-bentonite mixing rations.

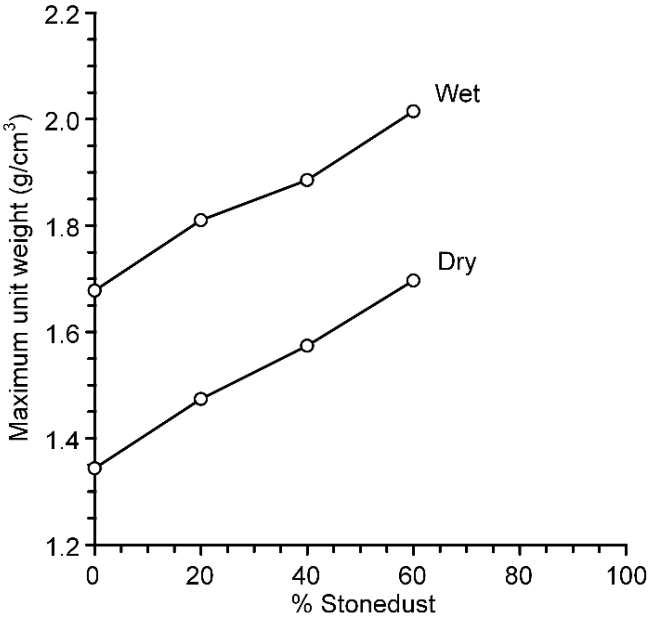

Figure 5.4 Maximum unit weight as a function of fine-grained stone dust-bentonite weight ratio comparing before and after compaction.

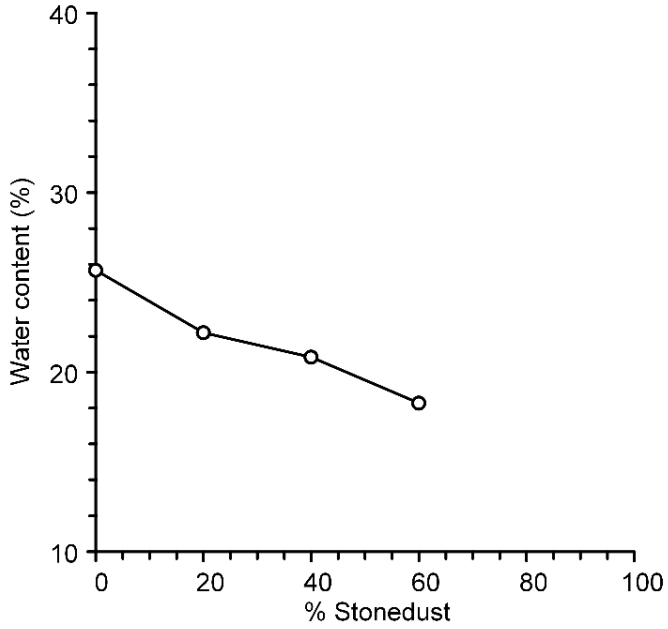

Figure 5.5 Optimum water content as a function of fine-grained stone dust-bentonite weight ratio.

Table 5.1 Compaction test results.

Fine grained stone dust: Bentonite (SD:B)			
Weight ratio (SD:B)	Sample No.	Maximum dry densities (g/cc)	Optimum water contents (%)
0:100	SD-0	1.34	25.67
20:80	SD-20	1.47	22.20
40:60	SD-40	1.57	20.83
60:40	SD-60	1.70	18.27

5.3 Direct Shear test

5.3.1 Test method

A direct shear test is conducted to determine the peak shear strength of the compacted specimens comprised of bentonite mixed with fine-grained stone dust. The compaction process utilizes the optimum water content for each specimen. Following compaction, the specimens are trimmed using a soil trimmer before being placed within a dedicated stainless steel shear box (Figure 5.6). A hydraulic load cell facilitates the application of constant normal stresses in stages of 25 psi, 50 psi, 75 psi,

and 100 psi. Shear stress is then applied, and both the shear displacement and dilation are meticulously recorded at intervals of 0.01 mm.

5.3.2 Test results

The shear stresses in terms of shear displacement are shown in Figure 5.7. The result show trend of increasing shear stresses with increasing shear displacement, particularly evident under high normal stress conditions. Additionally, the figure demonstrates a significant correlation between increasing aggregate particle size and the magnitude of dilatation observed.

Specimens with lower bentonite percentages exhibited greater shear strengths compared to those with higher bentonite content. The relationships between cohesion and friction angle for the various mixtures are shown in Figure 5.9. The data suggests that an increase in the fine-grained stone dust content leads to a decrease in cohesion (c). While a reduction in the bentonite percentage results in an increase in friction angle (ϕ). This trend can potentially be attributed to the enhanced frictional resistance between the grain surfaces within the stone dust mixture.

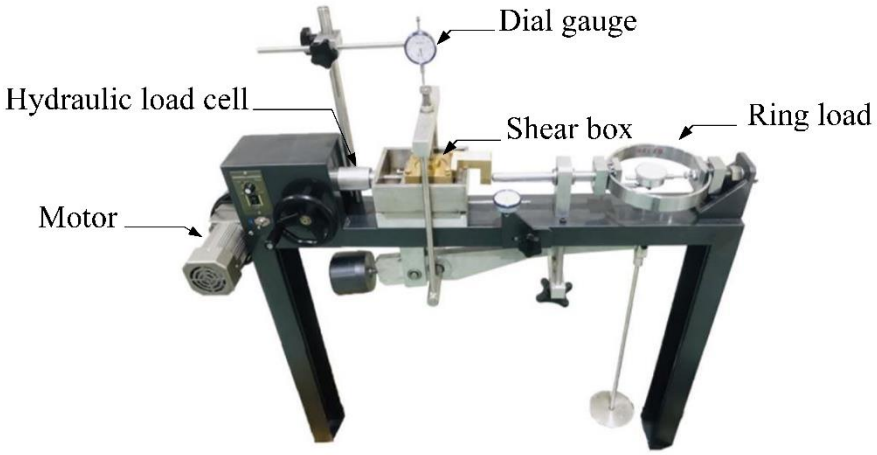

Figure 5.6 Direct shear device of fined-aggregates stone dust-mixed bentonite testing using by direct shear machine.

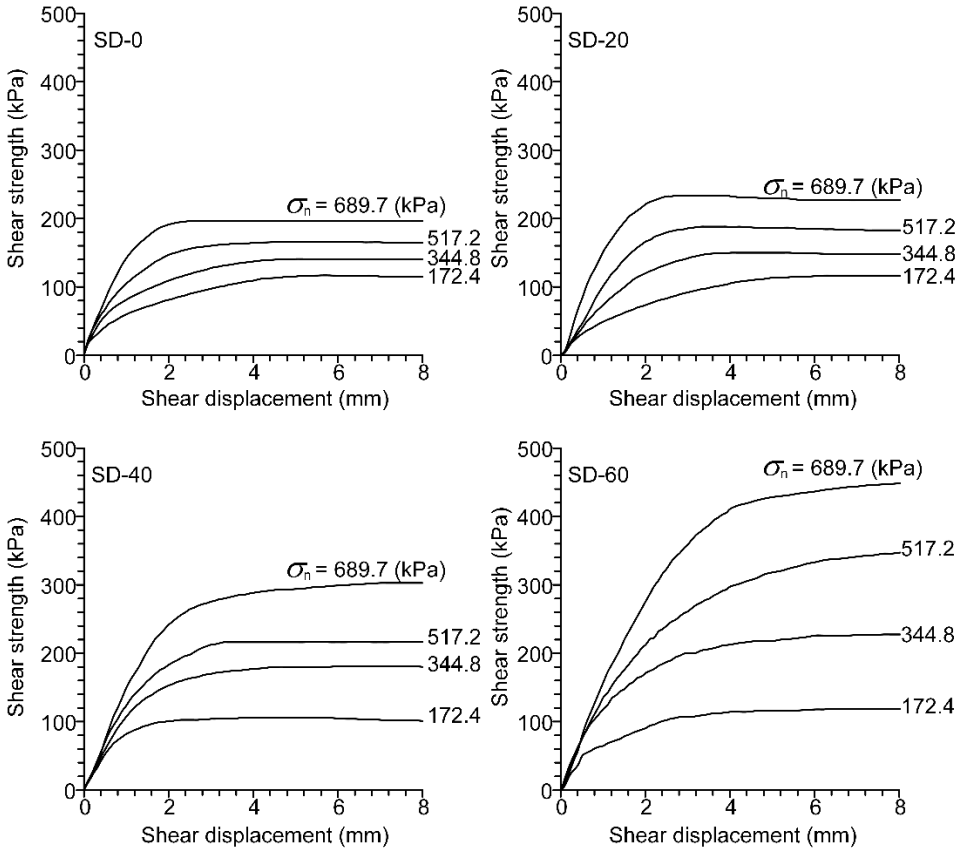

Figure 5.7 Shear stress as a function of shear displacement of fine-grained stone dust-bentonite mixtures.

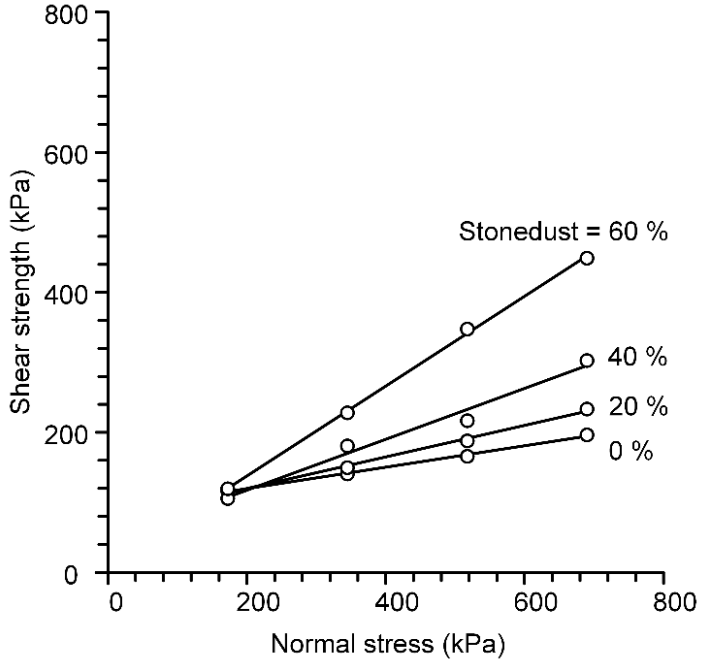

Figure 5.8 Shear strengths as a function normal stress.

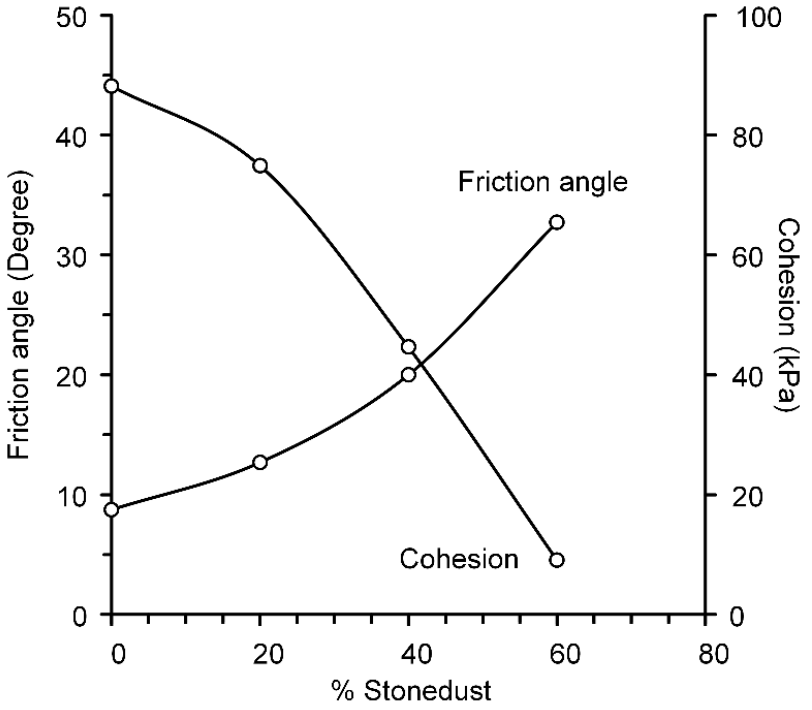

Figure 5.9 The cohesions and friction angles of specimens mixtures for the first separator (set I).

Table 5.2 Direct shear test results of fine-grained stone dust-bentonite mixtures results.

Fine grained stone dust: Bentonite (SD:B)			
Weight ratio	Sample No.	C (kPa)	Friction angles (ϕ)
0:100	SD-0	88.2	9
20:80	SD-20	74.9	13
40:60	SD-40	44.7	20
60:40	SD-60	9.1	33

5.4 Consolidation test

5.4.1 Test method

Consolidation tests are conducted on the prepared mixtures using their previously determined optimum water content. Constant axial stresses are applied via a hydraulic load cell (Figure 5.10). The applied axial stresses encompassed a range from 10 kPa to 1280 kPa in increments of 10, 20, 40, 80, 160, 320, 640, and 1280 kPa. Each test is maintained for a duration of 10 days under ambient temperature conditions. High-precision gauges are employed to record the axial displacements throughout the testing process.

Figure 5.10 Consolidation testing of fined-aggregates stone dust-mixed bentonite testing using by Soil test pro machine.

5.4.2 Test results

The relationship between the void ratio and the effective stress shows downward trends when increasing percentages of fined grained stone dust. The cumulative pore volume decreases with increasing fined grained stone dust percentage as shown in Figure 5.11. The settlement of fine-grained stone dust-bentonite mixtures decreases when the fined grained stone dust contents increase. This could be the pore filling phenomena, which occurs with addition of bentonite particles to fine grained stone dust. The bentonite particles can penetrate inside the void spaces created by the fined grained stone dust, which stiffens the specimens matrix.

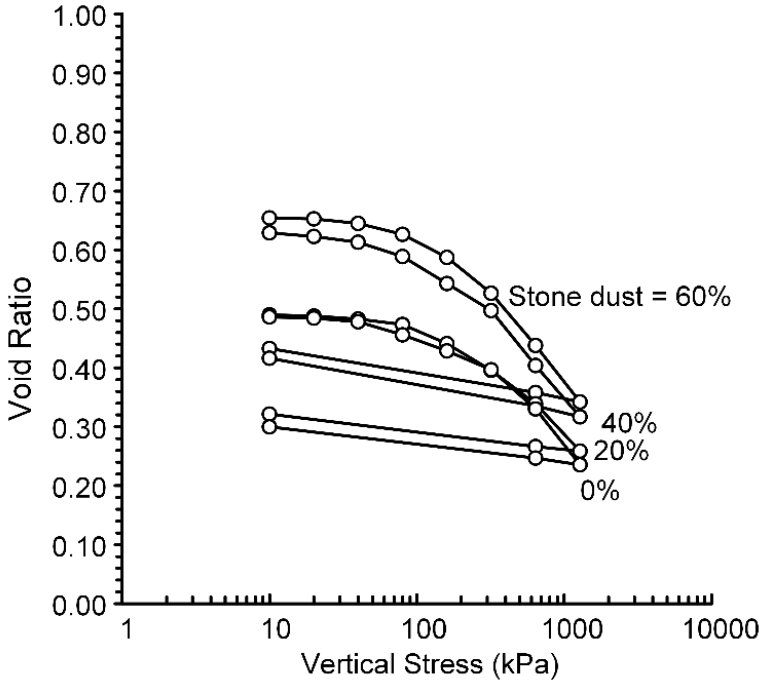

Figure 5.11 Void ratio as a function of effective stress of fine-grained stone dust-bentonite mixtures.

5.5 Swelling test

5.5.1 Swelling tests under different bentonite weight ratios

5.5.1.1 Test method

This study explores the influence of varying weight ratios between fine-grained stone dust and bentonite. The weight ratios studied include 0:100, 20:80, 40:60, and 60:40. Each sample is compacted within a mold in five layers, receiving a total of 27 compaction cycles. Following compaction, the top surface is carefully trimmed to ensure a smooth finish. A porous brass disc is then placed on top of the sample (Figure 5.12). Subsequently, the sample is submerged underwater for testing. During the initial 30 minutes of the test, readings are recorded at one-minute intervals. Following this initial period, the reading frequency gradually increased to hourly intervals. The swelling test method employed adheres to the ASTM D4546-08 standard practice.

5.5.1.2 Test results

Swelling ratio for various bentonite weight ratios are shown in Figure 5.13. The results indicated that the maximum swelling ratio increases with increasing bentonite weight ratio. This is because bentonite characteristically swells when contacts with water. Underwater the swelling increases rapidly within the 6 days, except for the samples with stone dust ratio of 0:100 and 20:80. They fluctuate until 10 days and tend to remain constant for all weight ratios after 30 days under water.

Figure 5.12 Swelling test setup in compaction mold.

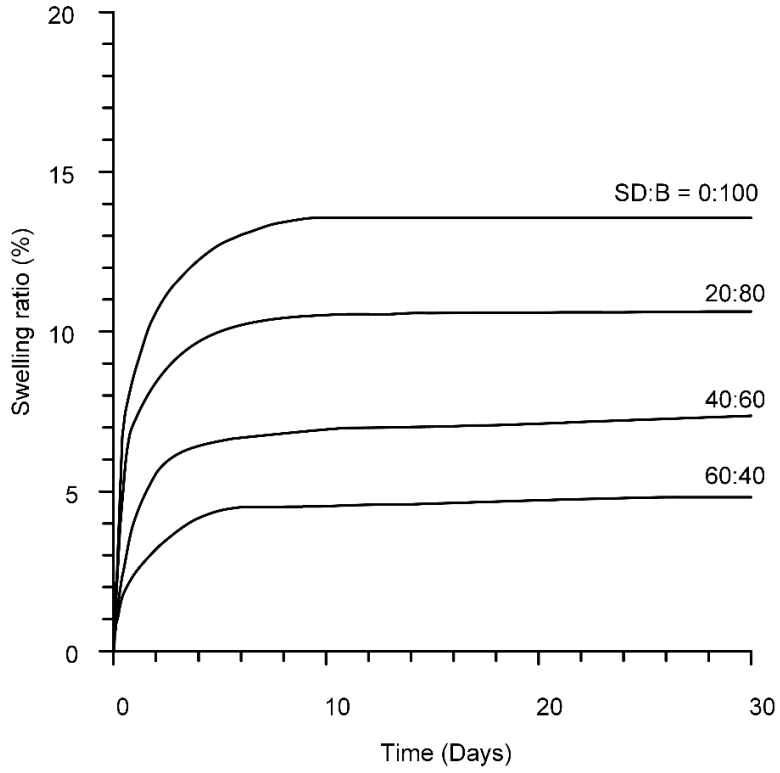

Figure 5.13 Swelling ratio as a function of time.

5.5.2 Swelling test under different constant loads

5.5.2.1 Test method

Specimens prepared with varying bentonite weight ratios are conducted under static loading conditions. Specimens are subjected to constant vertical loads of 2, 4, and 6 kilograms. In accordance with ASTM D4546-08, a consistent supply of water is maintained for the specimens throughout the 15-day testing period. The vertical swelling deformation is monitored at one-minute intervals during the initial 30 minutes of the test. Thereafter, the reading frequency gradually increased to hourly intervals.

5.5.2.2 Test results

The swelling ratios as a function of time under 2, 4 and 6 kg loading are shown in Figure 5.14. Figure 5.15 show the swelling behavior of the compacted fine-grained stone dust-bentonite mixtures under various constant loading conditions. The results suggest an inverse relationship between swelling ratio and applied static load. This observation can potentially be attributed to the influence of vertical stress on the internal structures of the compacted specimens. An increase in vertical stress may lead to a compaction of the spaces between aggregates, thereby reducing the potential for swelling strain.

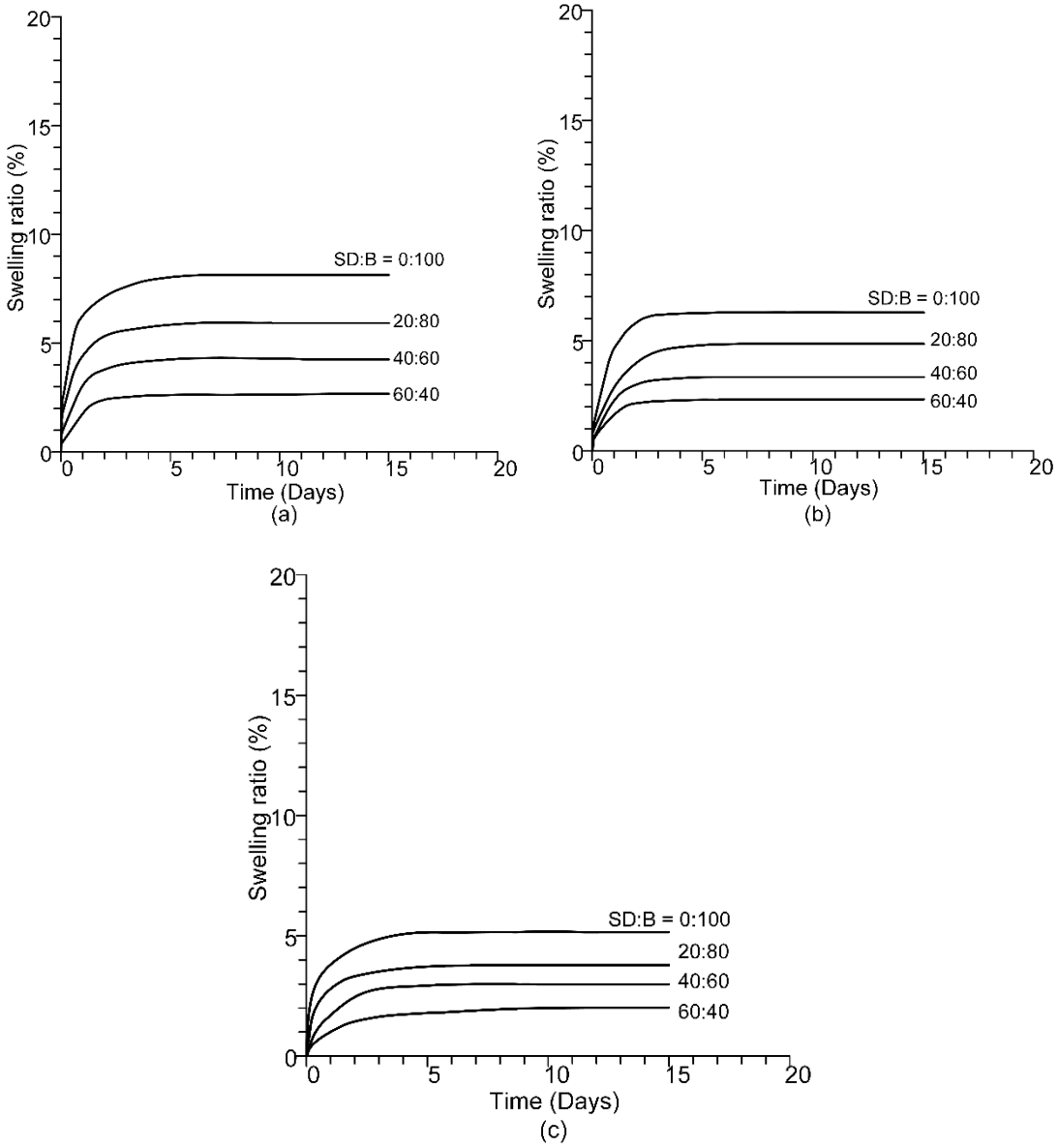

Figure 5.14 Swelling ratios of fined grained stone dust-bentonite mixtures as a function of time under loads of 2 kg (a), 4 kg (b) and 6 kg (c).

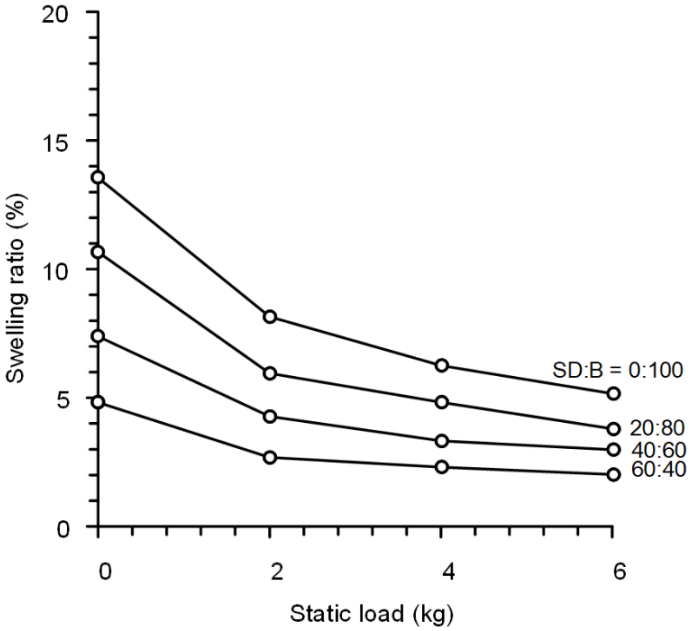

Figure 5.15 Swelling ratios of fined grained stone dust-bentonite mixtures as a function of static load.

5.6 Permeability test under falling head

The primary objective of the falling head tests is to determine the permeability of stone dust. The test uses stone dust particles smaller than 0.25 mm, categorized into three sizes: 0.25 mm, 0.15 mm, and 0.075 mm.

5.6.1 Test method

The hydraulic conductivity of the specimens is determined using a permeability test apparatus. The test setup employs standpipes with diameters of 6 mm, 10 mm, and 13 mm to facilitate the calculation of the internal cross-sectional area. Water from the standpipe is permitted to flow through the sample contained within a mold having a diameter of 101 mm and a length of 122 mm. To minimize potential water leakage along the sides of the cell, a thin layer of grease is applied to the inner surfaces of the mold. In order to reduce the presence of air voids, the test material is thoroughly compacted using a rammer device in three layers of approximately equal heights. Two filter papers are placed at the interface between the upper and lower portions of the tested material. During the testing process, the initial water level within the standpipe is designated as h_1. The water is then allowed to flow freely, and the time taken for the water level in the standpipe to reach h2 is

measured. It's important to note that the total head difference, which drives the water flow through the soil sample, varies throughout the test from h_1 to h_2 (Figure 5.16). The collected data is subsequently employed to calculate the hydraulic conductivity value (k), which can be determined using Darcy's Law as follows:

$$k=2.3\frac{a_m L}{At}\log\left(\frac{h_1}{h_2}\right) \tag{5.1}$$

where a is internal cross-sectional area of standpipe, L is length of soil sample, or the distance water flows through the soil mass during the experiment, A is sample area, in the direction perpendicular to water flow, t is time for the water in the standpipe to decrease from level h_1 (initial water level) to level h_2 (final water level) at time t, h_1 represents the energy difference driving water flow through the sample at the start of the test timer, h_2 represents the energy difference causing water to flow through the sample at the end of the test at time t.

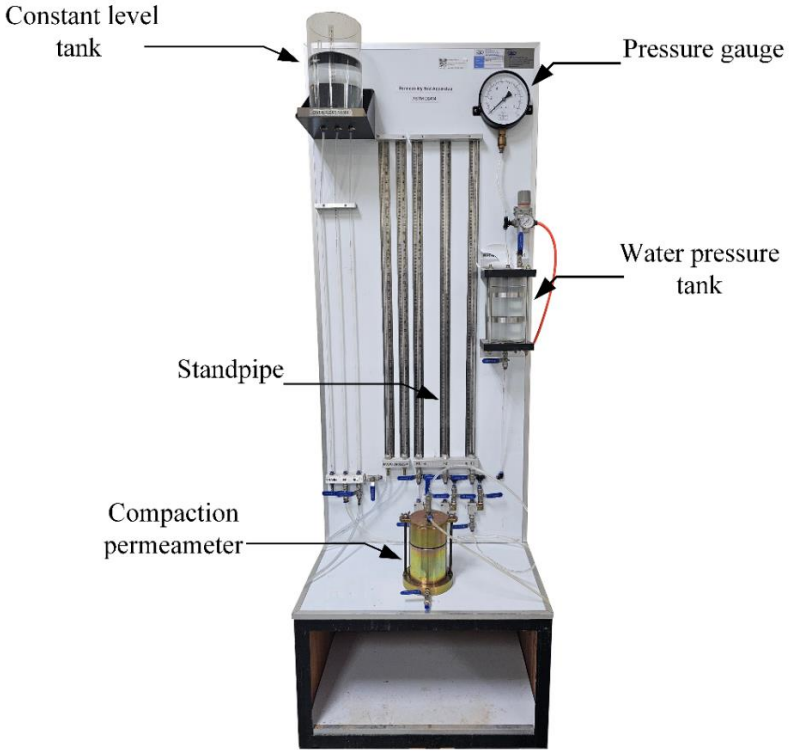

Figure 5.16 Permeability test apparatus of stone dust under falling head.

5.6.3 Test results

The results show that the grain size of 0.25 mm exhibits the highest flow rate, with a permeability coefficient (k) of 7.19×10^{-4} cm/s. This is significantly higher than the k values for the other grain sizes. In contrast, the grain size of 0.075 mm has the slowest flow rate, with a k value of 2.32×10^{-4} cm/s. This finding is consistent with the theoretical expectation that finer materials with smaller pores have lower permeability. All test results are shown in Table. 5.3 and Figure 5.17

An analysis of the results demonstrated a clear correlation between grain size and permeability. As the grain size increases from 0.075 mm to 0.25 mm, the permeability coefficient (k) also increases significantly. This trend is consistent with the theoretical understanding of permeability, where larger pores facilitate faster flow of fluids. However, when grain size of more than 0.25 mm, the increase in permeability is less pronounced.

Table 5.3 Test results of permeability under falling head of each particle sizes.

Grains size 0.25 mm								
Test No.	Manometers		Head, h (cm)	t (s)	A_m (cm^2)	k_t (cm/s)	η_t/η_{20}	k_{20} (cm/s)
	h_1	h_2						
1	80.0	70.0	10.0	18.0	0.28	3.15E-04	0.906	2.86×10^{-4}
2	80.0	70.0	10.0	46.0	0.79	3.43E-04	0.906	3.11×10^{-4}
3	30.0	20.0	10.0	54.0	1.33	1.50E-03	0.906	1.36×10^{-3}
Average Coefficient of Permeability, k_t is 7.19×10^{-4} cm/sec								
Average Coefficient of Permeability, k_{20} is 6.51×10^{-4} cm/sec								
Grains size 0.15 mm								
Test No.	Manometers		Head, h (cm)	t (s)	A_m (cm^2)	k_t (cm/s)	η_t/η_{20}	k_{20} (cm/s)
	h_1	h_2						
1	50.0	40.0	10.0	47	0.28	2.02×10^{-4}	0.906	1.83×10^{-4}
2	50.0	40.0	10.0	90	0.79	2.93×10^{-4}	0.906	2.65×10^{-4}
3	50.0	40.0	10.0	144	1.33	3.09×10^{-4}	0.906	2.80×10^{-4}
Average Coefficient of Permeability, k_t is 2.68×10^{-4} cm/sec								
Average Coefficient of Permeability, k_{20} is 2.43×10^{-4} cm/sec								
Grains size 0.075 mm								
Test No.	Manometers		Head, h (cm)	t (s)	A_m (cm^2)	k_t (cm/s)	η_t/η_{20}	k_{20} (cm/s)
	h_1	h_2						
1	50.0	40.0	10.0	72	0.28	1.32×10^{-4}	0.906	1.19×10^{-4}
2	50.0	40.0	10.0	120	0.79	2.20×10^{-4}	0.906	1.99×10^{-4}
3	45.0	35.0	10.0	146	1.33	3.44×10^{-4}	0.906	3.11×10^{-4}
Average Coefficient of Permeability, k_t is 2.32×10^{-4} cm/sec								
Average Coefficient of Permeability, k_{20} is 2.10×10^{-4} cm/sec								

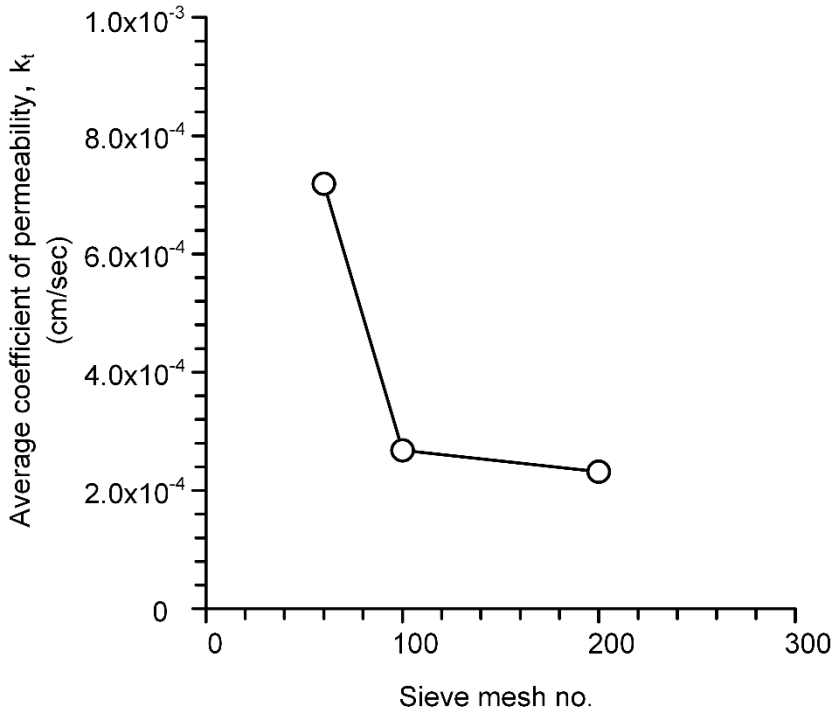

Figure 5.17 Average coefficient of permeability of each sieve mesh no.